

ECON: Explicit Clothed humans Obtained from Normals

Yuliang Xiu¹ Jinlong Yang¹ Xu Cao² Dimitrios Tzionas³ Michael J. Black¹

¹Max Planck Institute for Intelligent Systems, Tübingen, Germany

²Osaka University, Japan ³University of Amsterdam, the Netherlands

{yuliang.xiu, jinlong.yang, black}@tue.mpg.de cao.xu@ist.osaka-u.ac.jp d.tzionas@uva.nl

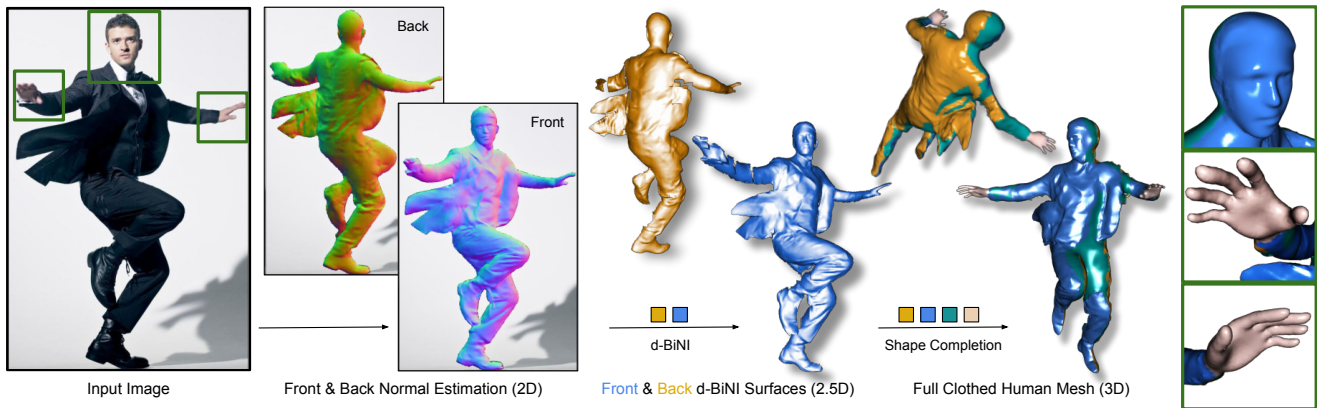


Figure 1. **Human digitization from a color image.** ECON combines the best aspects of implicit and explicit surfaces to infer high-fidelity 3D humans, even with loose clothing or in challenging poses. It does so in three steps: (1) It infers detailed 2D normal maps for the front and back side (Sec. 3.1). (2) The normal maps are converted into detailed, yet incomplete, 2.5D **front** and **back** surfaces guided by a SMPL-X estimate (Sec. 3.2). (3) It then “inpaints” the **missing geometry** between two surfaces (Sec. 3.3). If the **face or hands** are noisy, they can optionally be replaced with the ones from SMPL-X, which have a cleaner geometry. See the [video on our website](#) for more results.

Abstract

The combination of deep learning, artist-curated scans, and Implicit Functions (IF), is enabling the creation of detailed, clothed, 3D humans from images. However, existing methods are far from perfect. IF-based methods recover free-form geometry, but produce disembodied limbs or degenerate shapes for unseen poses or clothes. To increase robustness for these cases, existing work uses an explicit parametric body model to constrain surface reconstruction, but this limits the recovery of free-form surfaces such as loose clothing that deviates from the body. What we want is a method that combines the best properties of implicit and explicit methods. To this end, we make two key observations: (1) current networks are better at inferring detailed 2D maps than full-3D surfaces, and (2) a parametric model can be seen as a “canvas” for stitching together detailed surface patches. Based on these, our method, ECON, has three main steps: (1) It infers detailed 2D normal maps for the front and back side of a clothed person. (2) From these, it recovers 2.5D front and back surfaces, called d-BiNI, that are equally detailed, yet incomplete, and registers these w.r.t. each other with the help of a SMPL-X body mesh recovered from the image. (3) It

“inpaints” the missing geometry between d-BiNI surfaces. If the face and hands are noisy, they can optionally be replaced with the ones of SMPL-X. As a result, ECON infers high-fidelity 3D humans even in loose clothes and challenging poses. This goes beyond previous methods. Quantitative evaluation on the CAPE and Renderpeople datasets shows that ECON is more accurate than the state of the art. Perceptual studies also show that ECON’s perceived realism is better by a large margin. Code and models are available for research purposes at xiuyuliang.cn/econ

1. Introduction

Human avatars will be key for future games and movies, mixed-reality, tele-presence and the “metaverse”. To build realistic and personalized avatars at scale, we need to faithfully reconstruct detailed 3D humans from color photos taken in the wild. This is still an open problem, due to its challenges; people wear all kinds of different clothing and accessories, and they pose their bodies in many, often imaginative, ways. A good reconstruction method must accurately capture these, while also being robust to novel clothing and poses.

Initial, promising, results have been made possible by using artist-curated scans as training data, and deep implicit functions (IF) [51, 54] as a 3D representation. Seminal work on PIFu [60] and PIFuHD [61] uses “pixel-aligned” IF and reconstructs detailed clothed 3D humans with unconstrained topology. However, these methods tend to overfit to the poses seen in the training data, and have no explicit knowledge about the human body’s structure. Consequently, they tend to produce disembodied limbs or degenerate shapes for images with unseen poses; see the second row of Fig. 2. Follow-up work [25, 67, 69, 75] accounts for such artifacts by regularizing the IF using a shape prior provided by an explicit body model [47, 55], but this can limit generalization to novel clothing while attenuating shape details; see the third and fourth rows of Fig. 2. In other words, there are trade-offs between robustness, generalization and detail.

What we want, however, is the *best of both worlds*, the robustness of explicit anthropomorphic body models, and the flexibility of IF to capture arbitrary topologies. To that end, we make two key observations: (1) While inferring detailed 2D normal maps from color images is relatively easy [29, 61, 67], inferring a 3D geometry with equally fine details is still challenging [11]. Thus, we exploit networks to infer detailed “geometry-aware” 2D maps that we then lift to 3D. (2) A body model can be seen as a low-frequency “canvas” that “guides” the stitching of detailed surface parts.

With these in mind, we develop ECON, a novel method for “Explicit Clothed humans Obtained from Normals”. ECON takes as input an RGB image and a SMPL-X body inferred from the image. Then, it outputs a 3D human in free-form clothing with a level of detail and robustness that goes beyond the state of the art (SOTA); see the bottom of Fig. 2. Specifically, ECON takes *three steps*.

Step 1: Front & back normal reconstruction. We predict front- and back-side clothed-human normal maps from the input RGB image, conditioned on the body estimate, with a standard image-to-image translation network.

Step 2: Front & back surface reconstruction. We take the previously predicted normal maps, and the corresponding depth maps that are rendered from the SMPL-X mesh, to produce detailed and coherent front-/back-side 3D surfaces, $\{\mathcal{M}_F, \mathcal{M}_B\}$. To this end, we extend the recent BiNI method [9], and develop a novel optimization scheme that is aimed at satisfying three goals for the resulting surfaces: (1) their high-frequency components agree with clothed-human normals, (2) their low-frequency components and the discontinuities agree with the SMPL-X ones, and (3) the depth values on their silhouettes are coherent with each other and consistent with the SMPL-X-based depth maps. The two output surfaces, $\{\mathcal{M}_F, \mathcal{M}_B\}$, are detailed yet incomplete, i.e., there is missing geometry in occluded and “profile” regions.

Step 3: Full 3D shape completion. This module takes two inputs: (1) the SMPL-X mesh, and (2) the two d-BiNI

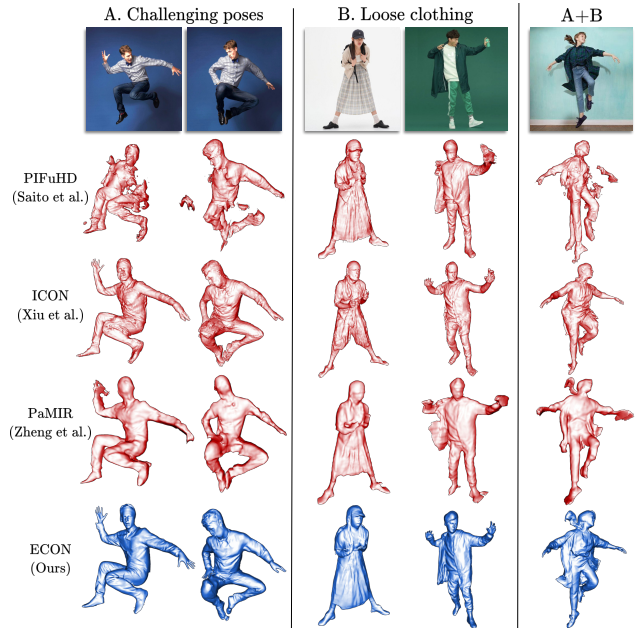


Figure 2. **Summary of SOTA.** PIFuHD recovers clothing details, but struggles with novel poses. ICON and PaMIR regularize shape to a body shape, but over-constrain the skirts, or over-smooth the wrinkles. ECON combines their best aspects.

surfaces, $\{\mathcal{M}_F, \mathcal{M}_B\}$. The goal is to “inpaint” the missing geometry. Existing methods struggle with this problem. On one hand, Poisson reconstruction [35] produces “blobby” shapes and naively “infills” holes without exploiting a shape distribution prior. On the other hand, data-driven approaches, such as IF-Nets [12], struggle with missing parts caused by (self-)occlusions, and lose details present in given high-quality surfaces, producing degenerate geometries.

We address above limitations in two steps: (1) We extend and re-train IF-Nets to be conditioned on the SMPL-X body, so that SMPL-X regularizes shape “infilling”. We discard the triangles that lie close to $\{\mathcal{M}_F, \mathcal{M}_B\}$, and keep the remaining ones as “infilling patches”. (2) We stitch together the front- and back-side surfaces and “infilling patches” via Poisson reconstruction; note that holes between these are small enough for a general purpose method. The result is a full 3D shape of a clothed human; see the bottom of Fig. 2.

We evaluate ECON both on established benchmarks (CAPE [50], Renderpeople [58]) and in-the-wild images. Quantitative analysis reveals that ECON outperforms SOTA. A perceptual study echos this, showing that ECON is significantly preferred over competitors on challenging poses and loose clothing, and competitive with PIFuHD on fashion images. Qualitative results show that ECON generalizes better than the SOTA to a wide variety of poses and clothing, even with extreme looseness or complex topology; see Fig. 7.

ECON combines the best aspects of explicit and implicit surfaces, to recover 3D clothed humans with a good level of detail and robustness. Code and models are available for research purposes at xiuyuliang.cn/econ

2. Related Work

Image-based clothed human reconstruction. Regarding geometric representation, we group the mainstream clothed human reconstruction approaches into two categories:

1) **Explicit-shape-based approaches** use either a mesh-based parametric body model [33, 47, 55, 59, 68], or a non-parametric depth map [21, 62], or point cloud [71] to reconstruct 3D humans. Many methods [14, 18, 34, 36–38, 41, 63, 72, 72] estimate or regress minimally-clothed 3D body meshes from RGB pixels and ignore clothing. To account for clothed human shapes, another line of work [2–5, 39, 56, 65, 78] adds 3D offsets on top of body mesh. This is compatible with current animation pipelines, as they inherit the hierarchical skeleton and skinning weights from the underlying statistical body model. However, this “body+offset” approach is not flexible enough to model loose clothing, which deviates significantly from the body topology, such as dresses and skirts. To increase topological flexibility, some methods [8, 31] reconstruct 3D clothed humans by identifying the type of clothing and using the appropriate model to reconstruct it. Scaling up this “cloth-aware” approach to many clothing styles is nontrivial, limiting generalization to in-the-wild outfit variation.

2) **Implicit-function-based approaches** are topology-agnostic and, thus, can be used to represent arbitrary 3D clothed human shapes. SMPLicit [15] and ClothWild [52] learn a generative clothing model with neural distance field [13, 51, 54] from a 3D clothing dataset. Given an image, the clothed human is reconstructed by estimating a parametric body and optimizing the latent space of the clothing model. However, the results usually do not align well with the image and lack geometric detail.

PIFu [60] introduces pixel-aligned implicit human shape reconstruction and PIFuHD [61] significantly improves the geometric details with a multi-level architecture and the normal maps predicted from the RGB image. However, these two methods do not exploit knowledge of the human body structure. Therefore, these methods overfit to the body poses in the training data, e.g. fashion pose, failing to generalize to unseen poses, thus producing non-human shapes with broken or disembodied limbs. To address these issues, several methods introduce different geometric priors to regularize the deep implicit representation: GeoPIFu [25] introduces a coarse shape of volumetric humans, Self-Portraits [45], PINA [17], and S3 [69] use depth or LIDAR information to regularize shape and improve robustness to pose variation.

Another direction leverages parametric body models, which represent human body shape well, model the kinematic structure of human body, and can be reliably estimated from the RGB images of clothed people. Such a representation can be viewed as a base shape upon which to model clothed humans. Therefore, several methods combine parametric body models with expressive implicit representations

to get the best of both worlds. PaMIR [75] and DeepMulti-Cap [74] condition the pixel-aligned features on a posed and voxelized SMPL mesh. JIFF introduces a 3DMM face prior to improve the realism of the facial region. ARCH [28] and ARCH++ [26] both use SMPL to unpose the pixel-aligned query points from a posed space to a canonical space. To further generalize to unseen poses on in-the-wild photos, ICON [67] regresses shapes from locally-queried features. However, the above approaches gain robustness to unseen poses at the cost of generalization ability to various, especially loose, clothing topologies. We argue that this is because loose clothing differs greatly from human body and that conditioning on the SMPL body in 3D makes it harder for networks to make full use of 2D image features.

Our work is also inspired by “sandwich-like” monocular reconstruction approaches, represented by Moduling Humans [21], FACSIMILE [62] and Any-Shot GIN [66]. Moduling Humans has two networks: a *generator* that estimates the visible (front) and invisible (back) depth maps from RGB images, and a *discriminator* that helps regularize the estimation via an adversarial loss. FACSIMILE further improves the geometric details by leveraging a normal loss, which is directly computed from depth estimates via differentiable layers. Recently, Any-Shot GIN generalizes the sandwich-like scheme to novel classes of objects. Given RGB images, it predicts front and back depth maps as well, and then exploits IF-Nets [12] for shape completion. We follow a similar path and extend it, to successfully reconstruct clothed human shapes with SOTA pose generalization, and better details from normal images.

3. Method

Given an RGB image, ECON first estimates front and back normal maps (Sec. 3.1), then converts them into front and back partial surfaces (Sec. 3.2), and finally “inpaints” the missing geometry with the help of IF-Nets+ (Sec. 3.3). See ECON’s overview in Fig. 3.

3.1. Detailed normal map prediction

Trained on abundant pairs of RGB images and normal images, a “front” normal map, $\hat{\mathcal{N}}_F^c$, can be accurately estimated from an RGB image using image-to-image translation networks, which has been demonstrated in PIFuHD [61] or ICON [67]. Both methods also infer a “back” normal map, $\hat{\mathcal{N}}_B^c$, from the image. But, the absence of image cues lead to over-smooth $\hat{\mathcal{N}}_B^c$. To address this, we finetune ICON’s back-side normal generator, \mathcal{G}^{N^b} , with additional MRF loss [64].

To guide the normal map prediction and make it robust to various body poses, ICON conditions the normal map prediction module on the body normal maps, \mathcal{N}^b , rendered from estimated body \mathcal{M}^b . Thus, it is important to accurately align the estimated body and clothing silhouette. Apart from the \mathcal{L}_{N_diff} and \mathcal{L}_{S_diff} used in ICON [67], we also apply 2D

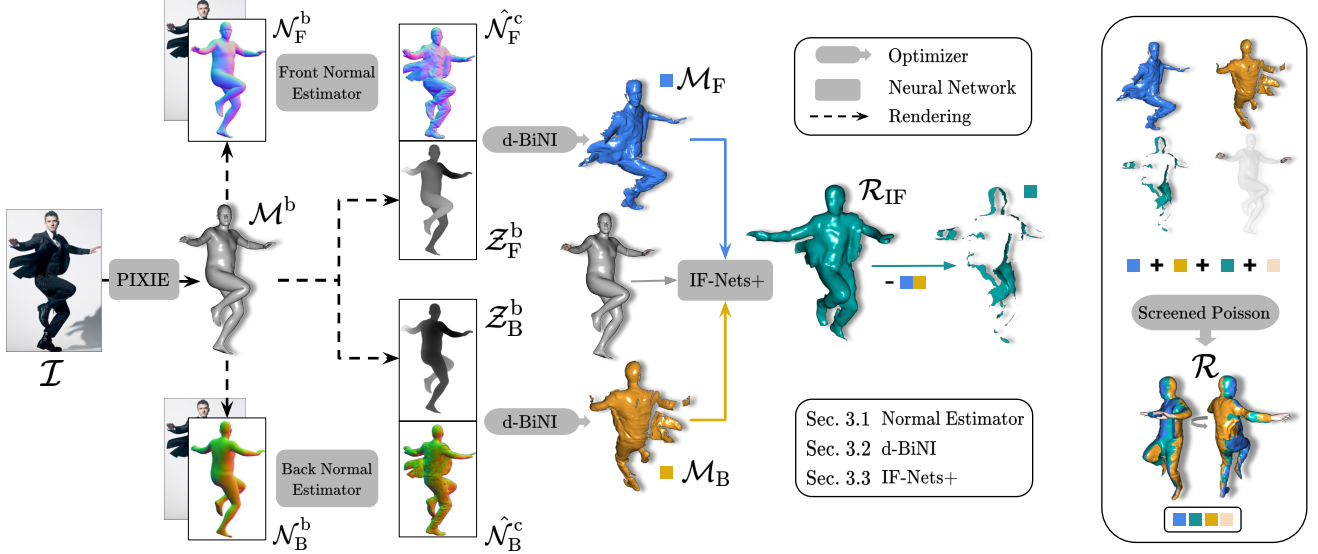


Figure 3. **Overview.** ECON takes as input an RGB image, \mathcal{I} , and a SMPL-X body, \mathcal{M}^b . Conditioned on the rendered front and back body normal images, \mathcal{N}^b , ECON first predicts front and back clothing normal maps, $\hat{\mathcal{N}}^c$. These two normals along with body depth maps, \mathcal{Z}^b , are fed into a d-BiNI optimizer to produce front and back surfaces, $\{\mathcal{M}_F, \mathcal{M}_B\}$. Based on such partial surfaces, and body estimate \mathcal{M}^b , IF-Nets+ implicitly completes \mathcal{R}_{IF} . With optional **face or hands** from \mathcal{M}^b , screened Poisson combines above all as final watertight \mathcal{R} .

body landmarks in an additional loss term $\mathcal{L}_{J,\text{diff}}$, to further optimize the SMPL-X body, \mathcal{M}^b , inferred from PIXIE [18]. Specifically, we optimize SMPL-X’s shape, β , pose, θ , and translation, t , to minimize:

$$\begin{aligned} \mathcal{L}_{\text{SMPL-X}} &= \mathcal{L}_{N,\text{diff}} + \mathcal{L}_{S,\text{diff}} + \mathcal{L}_{J,\text{diff}}, \\ \mathcal{L}_{J,\text{diff}} &= \lambda_{J,\text{diff}} |\mathcal{J}^b - \hat{\mathcal{J}}^c|, \end{aligned} \quad (1)$$

where $\mathcal{L}_{N,\text{diff}}$ and $\mathcal{L}_{S,\text{diff}}$ are the normal-map loss and silhouette loss introduced from ICON [67], and $\mathcal{L}_{J,\text{diff}}$ is the joint loss (L2) between 2D landmarks \mathcal{J}^c , which could be estimated by off-the-shell 2D pose estimator from the RGB image \mathcal{I} , and corresponding re-projected 2D joints \mathcal{J}^b from \mathcal{M}^b . For more implementation details, see [Sec. A.1](#) in Appx.

3.2. Front and back surface reconstruction

We now lift the clothed normal maps to 2.5D surfaces. We expect these 2.5D surfaces to satisfy three conditions: (1) high-frequency surface details agree with predicted clothed normal maps, (2) low-frequency surface variations, including discontinuities, agree with SMPL-X’s ones, and (3) the depth of front and back silhouettes are close to each other.

Unlike PIFuHD [61] or ICON [67], which train a neural network to regress the implicit surface from a clothed normal map, we explicitly model the depth-normal relationship using variational normal integration methods [9, 57]. Specifically, we tailor the recent bilateral normal integration (BiNI) method [9] to full-body mesh reconstruction by harnessing the coarse prior, depth maps, and silhouette consistency.

To satisfy the three conditions, we propose a depth-aware silhouette-consistent bilateral normal integration (d-BiNI)

method to jointly optimize for the front and back clothed depth maps, $\hat{\mathcal{Z}}_F^c$ and $\hat{\mathcal{Z}}_B^c$:

$$\text{d-BiNI}(\hat{\mathcal{N}}_F^c, \hat{\mathcal{N}}_B^c, \mathcal{Z}_F^b, \mathcal{Z}_B^b) \rightarrow \hat{\mathcal{Z}}_F^c, \hat{\mathcal{Z}}_B^c. \quad (2)$$

Here, $\hat{\mathcal{N}}_*^c$ is the front or back clothed normal map predicted by $\mathcal{G}^{\mathcal{N}^b}$ from $\{\mathcal{I}, \mathcal{N}^b\}$, and \mathcal{Z}_*^b is the front or back coarse body depth image rendered from the SMPL-X mesh, \mathcal{M}^b .

Specifically, our objective function consists of five terms:

$$\begin{aligned} \min_{\hat{\mathcal{Z}}_F^c, \hat{\mathcal{Z}}_B^c} & \mathcal{L}_n(\hat{\mathcal{Z}}_F^c; \hat{\mathcal{N}}_F^c) + \mathcal{L}_n(\hat{\mathcal{Z}}_B^c; \hat{\mathcal{N}}_B^c) + \\ & \lambda_d \mathcal{L}_d(\hat{\mathcal{Z}}_F^c; \mathcal{Z}_F^b) + \lambda_d \mathcal{L}_d(\hat{\mathcal{Z}}_B^c; \mathcal{Z}_B^b) + \\ & \lambda_s \mathcal{L}_s(\hat{\mathcal{Z}}_F^c, \hat{\mathcal{Z}}_B^c), \end{aligned} \quad (3)$$

where \mathcal{L}_n is front and back BiNI terms introduced by BiNI [9], \mathcal{L}_d is front and back depth prior terms, and \mathcal{L}_s is a front-back silhouette consistency term. For a more detailed discussion on these terms, see [Sec. A.2](#) in Appx.

With [Eq. \(3\)](#), we make two technical contributions beyond BiNI [9]. First, we use the coarse depth prior rendered from the SMPL-X body mesh, \mathcal{Z}_i^b , to regularize BiNI:

$$\mathcal{L}_d(\hat{\mathcal{Z}}_i^c; \mathcal{Z}_i^b) = |\hat{\mathcal{Z}}_i^c - \mathcal{Z}_i^b| \quad i \in \{F, B\}. \quad (4)$$

This addresses the key problem of putting the front and back surfaces together in a coherent way to form a full body. Optimizing BiNI terms \mathcal{L}_n remains an arbitrary global offset between front and back surfaces. The depth prior terms \mathcal{L}_d encourage the surfaces with undecided offsets to be consistent with the SMPL-X body. For further intuitions on \mathcal{L}_n and \mathcal{L}_d , see [Fig. A.3](#) and [Fig. A.4](#) in Appx.

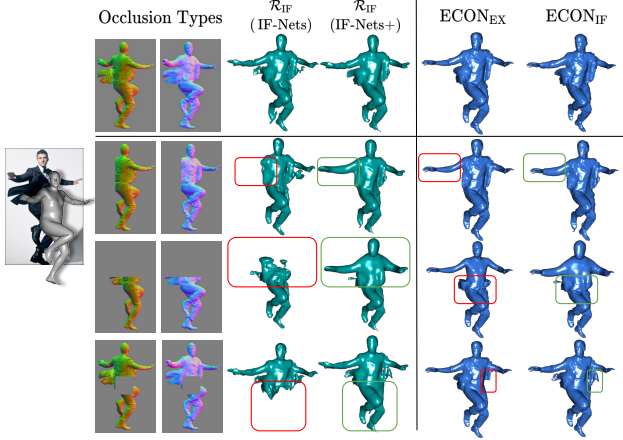


Figure 4. “Inpainting” the missing geometry. We simulate different cases of occlusion by masking the normal images and present the intermediate and final 3D reconstruction of different design choices. While IF-Nets misses certain body parts, IF-Nets+ produces a plausible overall shape. $ECON_{IF}$ produces more consistent clothing surfaces than $ECON_{EX}$ due to a learned shape distribution.

Second, we use a silhouette consistency term to encourage the front and back depth values to be the same at the silhouette boundary:

$$\mathcal{L}_s(\widehat{Z}_F^c, \widehat{Z}_B^c) = |\widehat{Z}_F^c - \widehat{Z}_B^c|_{\text{silhouette}}. \quad (5)$$

The silhouette term improves the physical consistency of the reconstructed front and back clothed depth maps. Without this term, d-BiNI produces intersections of the front and back surfaces around the silhouette, causing “blobby” artifacts and hurting reconstruction quality; see Fig. A.5 in Appx.

3.3. Human shape completion

For simple body poses without self-occlusions, merging front and back d-BiNI surfaces in a straight-forward way, as done in FACSIMILE [62] and Moduling Humans [21], can result in a complete 3D clothed scan. However, often poses result in self-occlusions, which cause large portions of the surfaces to be missing. In such cases, screened Poisson Surface Reconstruction (sPSR) [35] leads to blobby artifacts.

sPSR completion with SMPL-X ($ECON_{EX}$). A naive way to “infill” the missing surface is to make use of the estimated SMPL-X body. We remove the triangles from \mathcal{M}^b that are visible to front or back cameras. The remaining triangle “soup” $\mathcal{M}^{\text{cull}}$ contains both side-view boundaries and occluded regions. We apply sPSR [35] to the union of $\mathcal{M}^{\text{cull}}$ and d-BiNI surfaces $\{\mathcal{M}_F, \mathcal{M}_B\}$ to obtain a watertight reconstruction \mathcal{R} . This approach is denoted as $ECON_{EX}$. Although $ECON_{EX}$ avoids missing limbs or sides, it does not produce a coherent surface for the originally missing clothing and hair surfaces because of the discrepancy between SMPL-X and actual clothing or hair; see $ECON_{EX}$ in Fig. 4.

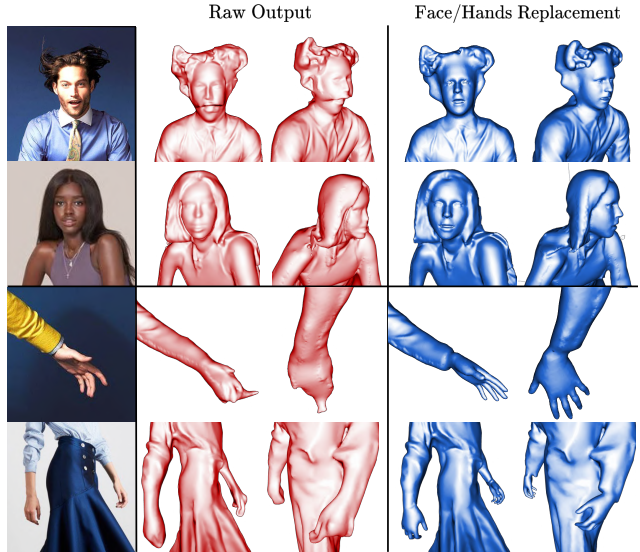


Figure 5. **Face and hand details.** The face and hands of the raw reconstruction can be replaced with the ones of the SMPL-X body.

Inpainting with IF-Nets+ (\mathcal{R}_{IF}). To improve reconstruction coherence, we use a learned implicit-function (IF) model to “inpaint” the missing geometry given front and back d-BiNI surfaces. Specifically, we tailor a general-purpose shape completion method, IF-Nets [12], to a SMPL-X-guided one, denoted as IF-Nets+. IF-Nets [12] completes the 3D shape from a deficient 3D input, such as an incomplete 3D human shape or a low-resolution voxel grid. Inspired by Li et al. [42], we adapt IF-Nets by conditioning it on a voxelized SMPL-X body to deal with pose variation; for details see Sec. A.3 in Appx. IF-Nets+ is trained on voxelized front and back ground-truth clothed depth maps, $\{Z_F^c, Z_B^c\}$, and a voxelized (estimated) body mesh, \mathcal{M}^b , as input, and is supervised with ground-truth 3D shapes. During training, we randomly mask $\{Z_F^c, Z_B^c\}$ for robustness to occlusions. During inference, we feed the estimated $\widehat{Z}_F^c, \widehat{Z}_B^c$ and \mathcal{M}^b into IF-Nets+ to obtain an occupancy field, from which we extract the inpainted mesh, \mathcal{R}_{IF} , with Marching cubes [48].

sPSR completion with SMPL-X and \mathcal{R}_{IF} ($ECON_{IF}$). To obtain our final mesh, \mathcal{R} , we apply sPSR to stitch (1) d-BiNI surfaces, (2) sided and occluded triangle soup $\mathcal{M}^{\text{cull}}$ from \mathcal{R}_{IF} , and optionally, (3) face or hands cropped from the estimated SMPL-X body. Although \mathcal{R}_{IF} is already a complete human mesh, we only use its side and occluded parts because its front and back regions lack sharp details compared to d-BiNI surfaces. This is due to the lossy voxelization of inputs and limited resolution of Marching cubes; see the local difference between $ECON_{\{IF, EX\}}$ and \mathcal{R}_{IF} in Fig. 4. Further, we use the face or hands cropped from \mathcal{M}^b because these parts are often poorly reconstructed in \mathcal{R}_{IF} , see difference in Fig. 5. The approach is denoted as $ECON_{IF}$.

4. Experiments

4.1. Datasets

Training on THuman2.0. THuman2.0 [70] contains 525 high-quality human textured scans in various poses, which are captured by a dense DSLR rig, along with their corresponding SMPL-X fits. We use THuman2.0 to train ICON’s variants, IF-Nets+, IF-Nets, PIFu and PaMIR.

Quantitative evaluation on CAPE & Renderpeople. We primarily evaluate on CAPE [50] and Renderpeople [58]. Specifically, we use the “CAPE-NFP” set (100 scans), which is used by ICON to analyze the robustness on complex human poses. Moreover, we select another 100 scans from Renderpeople, containing loose clothing, such as dresses, skirts, robes, down jackets, costumes, etc. With such clothing variance, Renderpeople helps numerically evaluate the flexibility of reconstruction methods w.r.t. shape topology. Samples of the two datasets are shown in Fig. 6.



Figure 6. **Datasets for numerical evaluation.** We evaluate ECON on images with unseen poses (left) and unseen outfits (right) on CAPE [50] and Renderpeople [58] datasets, respectively.

4.2. Metrics

Metrics for coarse geometric errors. We report the commonly used Chamfer distance (bi-directional point-to-surface) and P2S distance (1-directional point-to-surface) between ground-truth and reconstructed meshes, in cm.

Metric for fine geometric details. We report the L2 error between normal images rendered from reconstructed and ground-truth surfaces, by rotating a virtual camera around these by $\{0^\circ, 90^\circ, 180^\circ, 270^\circ\}$ w.r.t. to a frontal view.

4.3. Evaluation

Quantitative evaluation. We compare ECON with body-agnostic methods, i.e., PIFu [60] and PIFuHD [61], and body-aware methods, i.e., PaMIR [75] and ICON [67]; see in Tab. 1. For fair comparison, we use re-implementations of PIFu and PaMIR from ICON [67], because they have the same network settings and input data. ECON outperforms other methods by a large margin on images containing out-of-distribution poses (CAPE), with a reconstruction error below 1cm. In terms of out-of-distribution outfits (Renderpeople), ECON performs on par with PaMIR, and much better than PIFuHD. When it comes to high-frequency details measured by normals, both variants of ECON (ECON_{IF}, ECON_{EX}), achieve SOTA performance in quantitative evaluation.

Methods	OOD poses (CAPE)			OOD outfits (Renderpeople)		
	Chamfer ↓	P2S ↓	Normals ↓	Chamfer ↓	P2S ↓	Normals ↓
w/o SMPL body prior						
PIFu *	1.722	1.548	0.0674	1.706	1.642	0.0709
PIFuHD [†]	3.767	3.591	0.0994	1.946	1.983	0.0658
w/ SMPL body prior						
PaMIR *	1.004	1.004	0.0421	1.334	1.486	0.0523
ICON	1.272	1.139	0.0605	1.510	1.653	0.0686
ECON _{EX}	0.837	0.829	0.0331	1.409	1.506	0.0521
ECON _{IF}	0.844	0.841	0.0332	1.384	1.455	0.0511

Table 1. **Evaluation against the state of the art.** All models use a resolution of 256 for marching cubes. *Method is re-implemented in ICON for a fair comparison in terms of network settings and training data. [†]Official model is trained on Renderpeople dataset.

	ICON [67]	PIFuHD [61]
Challenging poses	0.423	0.182
Loose clothing	0.213	0.457
Fashion images	0.335	0.519

Table 2. **Perceptual study.** Numbers denote the chance that participants prefer the reconstruction of a competing method over ECON for in-the-wild images. A value of 0.5 indicates equal preference. A value of < 0.5 favors ECON, while of > 0.5 favors competitors.

Perceptual study. We further evaluate ECON on in-the-wild photos. We divide the test images into three categories: “challenging poses”, “loose clothing”, and “fashion images”. Examples of challenging poses and loose clothing can be seen in Fig. 7. Fashion images contain common photos of online clothing shopping, for examples see Fig. 9.

Due to the lack of ground-truth geometry, we perform a perceptual study. Participants are asked to choose the reconstruction they perceive as more realistic, between a baseline method and ECON. We compute the chances that each baseline is preferred over ECON in Tab. 2.

As Tab. 2 shows, the result of perceptual study echos the quantitative evaluation. For images containing challenging poses, ECON is significantly preferred over PIFuHD and outperforms ICON. On images of people wearing loose clothing, ECON is preferred over ICON with a large margin and outperforms PIFuHD. The reasons for slight preference of PIFuHD over ECON on fashion images are discussed in Sec. 6. This proves that, ECON combines d-BiNI with a body prior in a highly effective way; on the one hand, it is robust to unseen poses, while on the other hand, it is capable of reconstructing loose clothing and geometric details, as reconstructed shape is not over-constrained to the topology of a SMPL-X body. Figure 2 visualizes some comparisons. For more examples, see Figs. A.6 to A.8 in Appx.

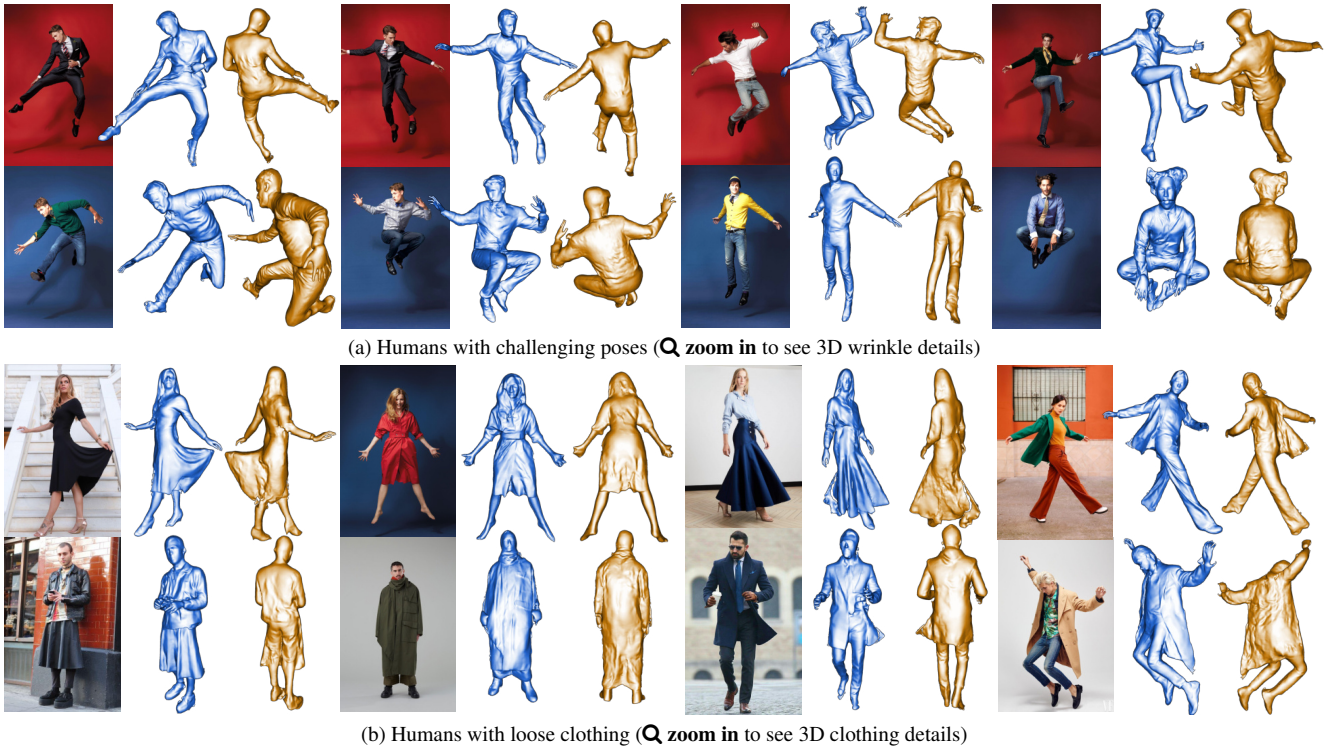


Figure 7. **Qualitative results on in-the-wild images.** We show 8 examples for reconstructing detailed clothed 3D humans from images with: (a) challenging poses and (b) loose clothing. For each example we show the input image along with two views (**front** and **rotated**) of the reconstructed 3D humans. Our approach is robust to pose variations, generalizes well to loose clothing, and contains detailed geometry.

Methods	OOD poses (CAPE [50])		OOD outfits (Renderpeople) [58]		Speed FPS \uparrow
	RMSE \downarrow	MAE \downarrow	RMSE \downarrow	MAE \downarrow	
BiNI [9]	27.64	21.11	20.61	16.07	0.52
d-BiNI	13.43	10.29	14.43	11.26	0.69

Table 3. **BiNI vs d-BiNI.** Comparison between BiNI and d-BiNI surfaces w.r.t. reconstruction accuracy and optimization speed.

4.4. Ablation study

d-BiNI vs BiNI. We compare d-BiNI with BiNI using 600 samples (200 scans \times 3 views) from CAPE and Renderpeople where ground-truth normal maps and meshes are available. We report in Tab. 3 the “root mean squared error” (RMSE) and “mean absolute error” (MAE) between estimated and rendered depth maps. d-BiNI significantly improves the reconstruction accuracy by about 50% compared to BiNI. This demonstrates the efficacy of using the coarse body mesh as regularization and taking the consistency of both front and back surface into consideration. Besides, d-BiNI accelerates the optimization by 33% than BiNI.

IF-Nets+ vs IF-Nets. Following the metrics of Sec. 4.2, we compare IF-Nets [12] with our IF-Nets+ on \mathcal{R}_{IF} . We show the quantitative comparison in Tab. 4. The improvement for out-of-distribution poses (“OOD poses”) shows that IF-Nets+ is more robust to pose variations than IF-Nets, as it is conditioned on the SMPL-X body. Figure 4 compares the geometry “inpainting” of both methods in case of occlusions.

Methods	OOD poses (CAPE)			OOD outfits (Renderpeople)		
	Chamfer \downarrow	P2S \downarrow	Normals \downarrow	Chamfer \downarrow	P2S \downarrow	Normals \downarrow
IF-Nets [12]	2.116	1.233	0.075	1.883	1.622	0.070
IF-Nets+	1.401	1.353	0.056	1.477	1.564	0.055
ECON _{IF}	0.844	0.841	0.033	1.384	1.455	0.051

Table 4. **Evaluation for shape completion.** Same metrics as Tab. 1, and ECON_{IF} is added as a reference.

5. Applications

Multi-person reconstruction. Thanks to the shape completion module, ECON can deal with occlusions. This makes it possible to reconstruct multiple persons from an image with inter-person occlusions, even though ECON has not been trained for this. Figure 8 shows three examples. The occluded parts, colored in red, are successfully recovered.

Detailed 3D humans for in-the-wild datasets. Datasets of real clothed humans with 3D ground truth [1, 6, 50, 58, 70, 76] are limited in size. In contrast, datasets of images without 3D ground truth are widely available in large sizes [20, 22, 46]. We can “augment” such datasets by reconstructing detailed 3D humans from their images. We apply ECON on SHHQ [20] and recover normal maps and 3D humans. Figure 9 shows some examples. As ECON-like methods mature, they could produce 3D pseudo ground truth from large-scale photos, to help people train pose regressors, or generate clothed avatars with details [7, 10, 23, 27, 32, 53, 73].

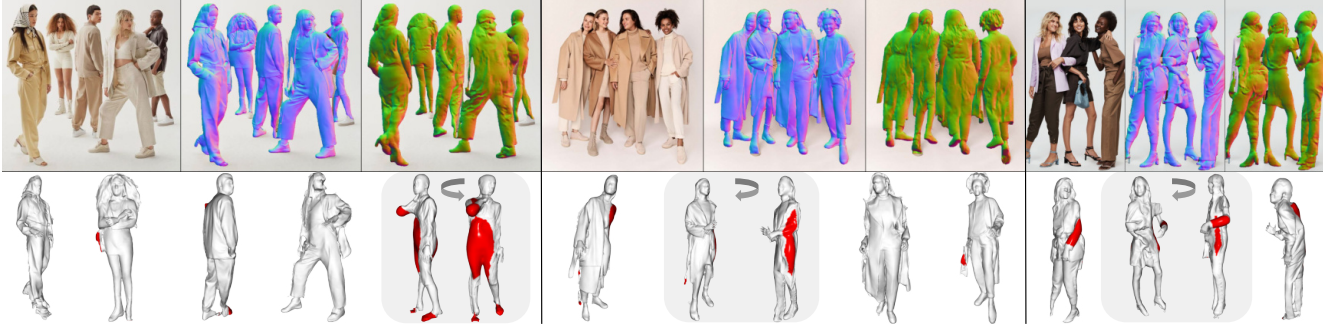


Figure 8. **Multiple humans with occlusions.** We detect humans from image, and apply ECON for each human separately. Although ECON is not designed for multiple persons, it is robust to inter-person occlusions. We show three examples, and for each: (top) input image and the predicted front and back normal maps, (bottom) ECON’s reconstruction. Red areas on the estimated mesh indicate occlusions.

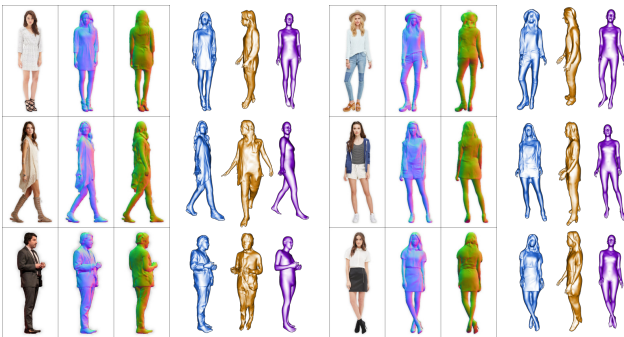


Figure 9. **SHHQ 3D reconstruction.** For each image we show a front and side view of ECON’s reconstruction and a SMPL-X fit.

6. Discussion

Limitations. ECON takes as input an RGB image and an estimated SMPL-X body. However, recovering SMPL-X bodies (or similar models) from a single image is still an open problem, and not fully solved. Any failure in this could lead to ECON failures, such as in Fig. 10-A and Fig. 10-B. The reconstruction quality of ECON primarily relies on the accuracy of predicted normal maps. Poor normal maps could result in overly close-by or even intersecting front and back surfaces, as shown in Fig. 10-C and Fig. 10-D.

Future work. Apart from addressing the above limitations, several other directions are useful for practical applications. Currently, ECON reconstructs only 3D geometry. One could additionally recover an underlying skeleton and skinning weights, e.g., with SSDR [40], to obtain fully-animatable avatars. Moreover, inferring back-view texture would result in fully-textured avatars. Disentangling clothing, hair, or accessories from the recovered geometry would enable the synthesis, editing and transfer of styles for these. Finally, ECON’s reconstructions could be useful as pseudo ground truth for training neural avatars [16, 19, 30].

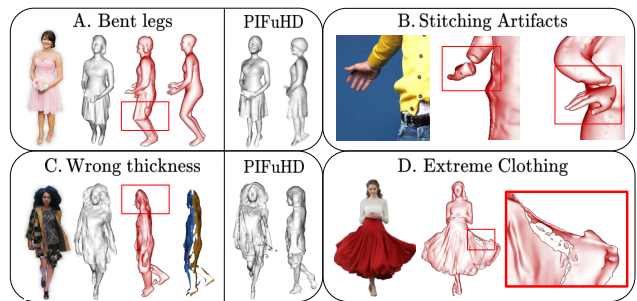


Figure 10. **Failure examples of ECON.** (A-B) Failures in recovering a SMPL-X body result, e.g., bent legs or wrong limb poses, cause ECON failures by extension. (C-D) Failures in normal-map estimation provide erroneous geometry to ECON to work with.

Possible negative impact. As the reconstruction matures, it opens the potential for low-cost realistic avatar creation. Although such a technique for sure benefits entertainment, film production, tele-presence and future metaverse applications, it could also facilitate deep-fake avatars. Regulations must be established to clarify the fair use of such technology.

7. Conclusion

We propose ECON, a method to reconstruct detailed clothed 3D humans from a color image. ECON combines the best of explicit parametric models and deep implicit functions; it estimates detailed 3D surfaces for the human body and clothing without being limited to specific topology, while being robust to challenging unseen poses and clothing. To this end, it employs the latest advances in variational normal integration and shape completion, and effectively extends these to the task of human reconstruction from color images. We believe this work can lead to both real-world applications and useful data augmentation for the 3D vision community, thus, we release our models and code.

Disclosure. MJB has received research gift funds from Adobe, Intel, Nvidia, Meta/Facebook, and Amazon. MJB has financial interests in Amazon, Datagen Technologies, and Meshcapade GmbH. While MJB is a part-time employee of Meshcapade, his research was performed solely at, and funded solely by, the Max Planck Society.

Acknowledgments. We thank Lea Hering and Radek Daněček for proofreading, Yao Feng, Haven Feng and Weiyang Liu for their feedback, and Tsvetelina Alexiadis for her help with the perceptual study. This project has received funding from the European Union’s Horizon 2020 research and innovation programme under the Marie Skłodowska-Curie grant agreement No.860768 (CLIFE project).

Appendices

In the following, we provide more details and discussion on normal prediction, d-BiNI and IF-Nets+, as well as more qualitative results in the perceptual study, as an extension of Sec. 3, Sec. 4 and Sec. 5 of the main paper. Please check the [video on our website](#) for an overview of the method and more results.

A. Implementation details

A.1. Normal map prediction

We set the loss weights $\lambda_{J,\text{diff}}$, $\lambda_{N,\text{diff}}$, and $\lambda_{S,\text{diff}}$ in Eq. (1) to 5.0, 1.0, and 1.0 respectively. However, if the overlap ratio between clothing and body mask is smaller than 0.5, it means humans are dressed with loose clothing. In this situation we trust the 2D joints more and increase the $\lambda_{J,\text{diff}} = 50.0$. Similarly, when the overlap between body mask inside the clothing mask and full body mask is smaller than 0.98, occlusion happens. In such cases we set $\lambda_{S,\text{diff}} = 0.0$ to avoid limb self-intersection after pose refinement.

During inference, following ICON [67], we iteratively refine SMPL-X and the predicted clothed-body normal maps for 50 interactions, with 1.10 iter/s speed on a Quadro RTX 5000 GPU. We use `rembg`¹ plus Mask R-CNN (ResNet50-FPN-V2) [24] for multi-person segmentation, `mediapipe` [49] to estimate full-body landmarks, `pypoisson`² for poisson reconstruction, and `MonoPort` [43, 44] for fast implicit surface query.

A.2. d-BiNI

Optimization details. To better present the optimization details, we first write the d-BiNI objective function in a

¹<https://github.com/danielgatis/rembg>

²<https://github.com/mmolero/pypoisson>

matrix form. Figure A.1 shows the four inputs to d-BiNI. We vectorize the front and back clothed and prior depth maps $\{\widehat{\mathbf{z}}_F^c, \widehat{\mathbf{z}}_B^c, \mathbf{z}_F^b, \mathbf{z}_B^b\}$ within Ω_n as $\{\widehat{\mathbf{z}}_F, \widehat{\mathbf{z}}_B, \mathbf{z}_F, \mathbf{z}_B\}$; all vectors are of length $|\Omega_n|$. d-BiNI then jointly solves for the front and back clothed depth $\widehat{\mathbf{z}}_F$ and $\widehat{\mathbf{z}}_B$ by minimizing the objective function consisting of the five terms:

$$\begin{aligned} \mathcal{L}(\widehat{\mathbf{z}}_F, \widehat{\mathbf{z}}_B) = & (\mathbf{A}_F \widehat{\mathbf{z}}_F - \mathbf{b}_F)^\top \mathbf{W}_F (\mathbf{A}_F \widehat{\mathbf{z}}_F - \mathbf{b}_F) \\ & + (\mathbf{A}_B \widehat{\mathbf{z}}_B - \mathbf{b}_B)^\top \mathbf{W}_B (\mathbf{A}_B \widehat{\mathbf{z}}_B - \mathbf{b}_B) \\ & + \lambda_d (\widehat{\mathbf{z}}_F - \mathbf{z}_F)^\top \mathbf{M} (\widehat{\mathbf{z}}_F - \mathbf{z}_F) \\ & + \lambda_d (\widehat{\mathbf{z}}_B - \mathbf{z}_B)^\top \mathbf{M} (\widehat{\mathbf{z}}_B - \mathbf{z}_B) \\ & + \lambda_s (\widehat{\mathbf{z}}_F - \widehat{\mathbf{z}}_B)^\top \mathbf{S} (\widehat{\mathbf{z}}_F - \widehat{\mathbf{z}}_B). \end{aligned} \quad (\text{A.1})$$

Here, $\mathbf{A}_F \in \mathbb{R}^{4|\Omega_n| \times |\Omega_n|}$ and $\mathbf{b}_F \in \mathbb{R}^{4|\Omega_n|}$ are constructed from the front normal map following Eq. (21) of BiNI [9]; \mathbf{A}_B and \mathbf{b}_B are from the back normal map. \mathbf{W}_F and $\mathbf{W}_B \in \mathbb{R}^{4|\Omega_n| \times 4|\Omega_n|}$ are bilateral weight matrices for front and back depth maps, respectively; both are constructed following Eq. (22) of BiNI [9] and depend on the unknown depth. \mathbf{M} and \mathbf{S} are $|\Omega_n| \times |\Omega_n|$ diagonal matrices whose diagonal entries indicate the pixels with depth priors and located at the silhouette, respectively. Specifically, the i -th diagonal entry m_i of \mathbf{M} is

$$m_i = \begin{cases} 1, & \text{if } i\text{-th entry of } \widehat{\mathbf{z}}_F \text{ in } \Omega_z \\ 0, & \text{otherwise} \end{cases}, \quad (\text{A.2})$$

while the i -th diagonal entry s_i of \mathbf{S} is

$$s_i = \begin{cases} 1, & \text{if } i\text{-th entry of } \widehat{\mathbf{z}}_F \text{ in } \partial\Omega_n \\ 0, & \text{otherwise} \end{cases}. \quad (\text{A.3})$$

Stacking $\widehat{\mathbf{z}}_F$ and $\widehat{\mathbf{z}}_B$ as $\widehat{\mathbf{z}} = \begin{bmatrix} \widehat{\mathbf{z}}_F \\ \widehat{\mathbf{z}}_B \end{bmatrix}$, Eq. (A.1) then reads

$$\begin{aligned} \mathcal{L}(\widehat{\mathbf{z}}) = & (\mathbf{A}\widehat{\mathbf{z}} - \mathbf{b})^\top \mathbf{W} (\mathbf{A}\widehat{\mathbf{z}} - \mathbf{b}) + \\ & \lambda_d (\widehat{\mathbf{z}} - \mathbf{z})^\top \widetilde{\mathbf{M}} (\widehat{\mathbf{z}} - \mathbf{z}) + \lambda_s \widehat{\mathbf{z}}^\top \widetilde{\mathbf{S}} \widehat{\mathbf{z}}, \end{aligned} \quad (\text{A.4})$$

where

$$\begin{aligned} \mathbf{A} = & \begin{bmatrix} \mathbf{A}_F & \\ & \mathbf{A}_B \end{bmatrix}, \quad \mathbf{b} = \begin{bmatrix} \mathbf{b}_F \\ \mathbf{b}_B \end{bmatrix}, \quad \mathbf{W} = \begin{bmatrix} \mathbf{W}_F & \\ & \mathbf{W}_B \end{bmatrix}, \\ \mathbf{z} = & \begin{bmatrix} \mathbf{z}_F \\ \mathbf{z}_B \end{bmatrix}, \quad \widetilde{\mathbf{M}} = \begin{bmatrix} \mathbf{M} & \\ & \mathbf{M} \end{bmatrix}, \quad \widetilde{\mathbf{S}} = \begin{bmatrix} \mathbf{S} & -\mathbf{S} \\ -\mathbf{S} & \mathbf{S} \end{bmatrix}. \end{aligned}$$

To minimize Eq. (A.4), we perform an iterative optimization similar to BiNI [9]. At each iteration, we first fix the weights \mathbf{W} and jointly solve for the front and back depth $\widehat{\mathbf{z}}$, then compute the new weights from the updated depth. When \mathbf{W} is fixed and treated as a constant matrix, solving for the depth becomes a convex least-squares problem. The

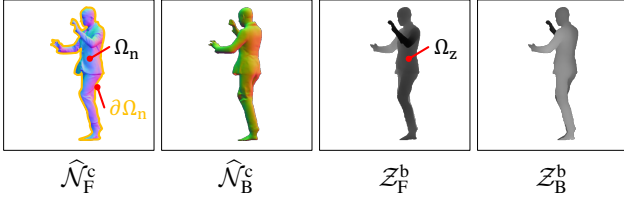


Figure A.1. The four inputs to d-BiNI. Ω_n is the domain of pixels where normal vectors are estimated and identical for front and back normal maps; Ω_z is where depth priors are rendered from the SMPL-X mesh and identical for front and back depth maps. Ω_n is, in general, different from Ω_z . $\partial\Omega_n$ is the silhouette of normal maps.

necessary condition for the global optimum is obtained by equating the gradient of Eq. (A.4) to 0:

$$(\mathbf{A}^\top \mathbf{W} \mathbf{A} + \lambda_d \widetilde{\mathbf{M}} + \lambda_s \widetilde{\mathbf{S}}) \widehat{\mathbf{z}} = \mathbf{A}^\top \mathbf{W} \mathbf{b} + \lambda_d \widetilde{\mathbf{M}} \mathbf{z}. \quad (\text{A.5})$$

Equation (A.5) is a large-scale sparse linear system with a symmetric positive definite coefficient matrix. We solve Eq. (A.5) using a CUDA-accelerated sparse conjugate gradient solver with a Jacobi preconditioner³.

Hyper-parameters. d-BiNI has three hyper-parameters: λ_d , λ_s , and k . λ_d and λ_s are used in the objective function Eq. (3), which control the influence of coarse depth prior term Eq. (4) and silhouette consistency term Eq. (5) separately. k is used in the original BiNI [9] to control the surface stiffness (See Sup.Mat-A in BiNI [9] for more explanation of k). Empirically, we set $\lambda_d = 1e^{-4}$, $\lambda_s = 1e^{-6}$, and $k = 2$.

Discussion of hyper-parameters. Figure A.3 shows the d-BiNI integration results under different values of k . It can be seen that a small k leads to tougher d-BiNI surfaces where discontinuities are not accurately recovered, while a large k softens the surface, and redundant discontinuities and noisy artifacts are introduced. Figure A.4 shows the effects of λ_d , which controls how much d-BiNI surfaces agree on the SMPL-X mesh. Small λ_d causes misalignment between the d-BiNI surface and the SMPL-X mesh, which will produce stitching artifacts. While an excessively large λ_d enforces d-BiNI to rely over heavily on SMPL-X, thus smoothing out the high-frequency details obtained from normals. Figure A.5 justifies the necessity of the silhouette consistency term. Without this term, the front and back d-BiNI surfaces intersect each other around the silhouettes, which will cause “blobby” artifacts after screened Poisson reconstruction [35].

A.3. IF-Nets+

Network structure. As Fig. A.2 shows, similar to IF-Nets [12], IF-Nets+ applies multi-scale voxel 3D CNN encoding on voxelized d-BiNI and the SMPL-X surface, namely $\mathcal{F}_1^{\text{d-BiNI}}$ and $\mathcal{F}_1^{\text{SMPL-X}}$,

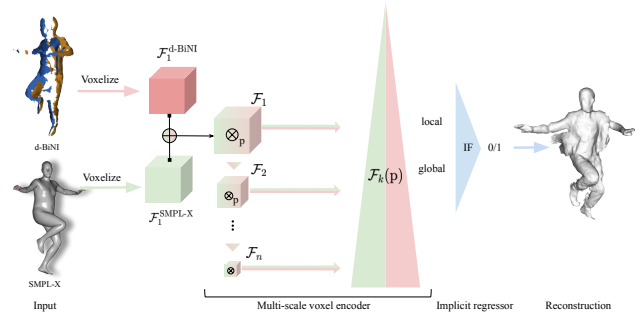


Figure A.2. Overview of IF-Nets+.

feature grids to account for both local and global information, $\mathcal{F}_1, \mathcal{F}_2, \dots, \mathcal{F}_n, \mathcal{F}_k \in \mathbb{R}^{K \times K \times K \times C_k}, n = 6$. These deep features are with decreasing resolution $K = \frac{N}{2^{k-1}}, N = 256$ and variable dimension channels $C = \{32, 32, 64, 128, 128, 128\}$. Following Li et al. [14], the positional embedding (N_freqs = 6) of query points is concatenated with multi-scale deep features to account for high-frequency details. All these features are then fed into an implicit function regressor, parameterized by a Multi-Layer Perceptron (MLP), to predict the occupancy value of point P. This MLP regressor is trained with BCE loss.

Training setting. IF-Nets and IF-Nets+ share the same training setting. The voxelization resolution for both SMPL-X and d-BiNI surfaces is 256^3 . We use RMSprop as an optimizer, with a learning rate $1e^{-4}$, and weight decay by a factor of 0.1 every 10 epochs. These networks are trained on an NVIDIA A100 for 20 epochs with a batch size of 48. Following ICON [67], we sampled 10000 points with the mixture of cube-uniform sampling and surface-around sampling, with standard deviation of 5cm.

Dataset details. We augment THuman2.0 [70] by (1) rotating the scans every 10 degrees around the yaw axis, to generate $525 \times 36 = 18900$ samples in total, and (2) randomly selecting a rectangle region from the d-BiNI depth maps, and erasing its pixels [77]. In particular, the erasing operation is being performed with $p = 0.8$ probability, the range of aspect ratio of erased area is between 0.3 and 3.3, and its range of proportion are $\{0.01, 0.05, 0.2\}$.

B. Qualitative results

Figures A.6 to A.8 show more comparisons used in our perceptual study, containing the results on in-the-wild images with challenging poses, loose clothing, and standard fashion poses, respectively. For each image, we display the results obtained by ECON, PIFuHD [61], and ICON [67] from the top to the bottom row. In each row, we show normal maps rendered in four views $\{0^\circ, 90^\circ, 180^\circ, 270^\circ\}$. The video on our website shows more reconstructions with a rotating virtual camera.

³<https://docs.cupy.dev/en/stable/reference/generated/cupy.scipy.sparse.linalg.cg.html>

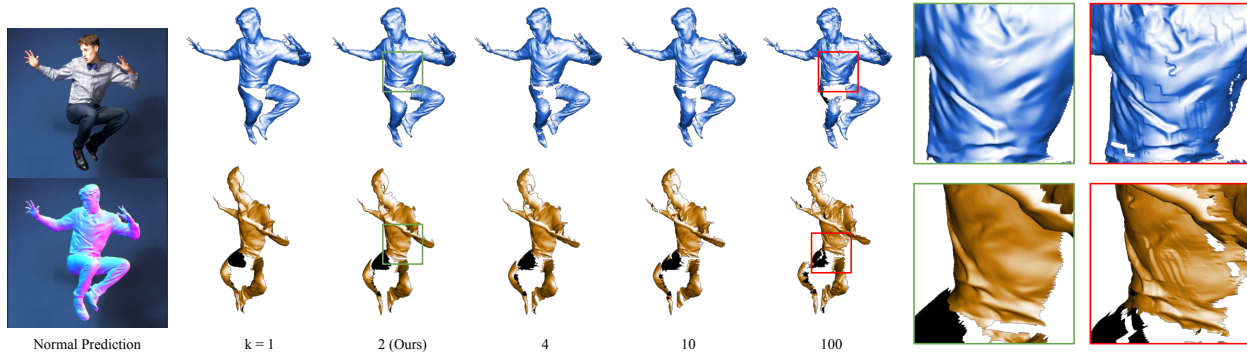


Figure A.3. **The effects of the hyper-parameter k on d-BiNI results.** k controls the stiffness of the target surface [9]. A smaller k leads to smooth d-BiNI surfaces, while a large k introduces unnecessary discontinuities and noise artifacts.

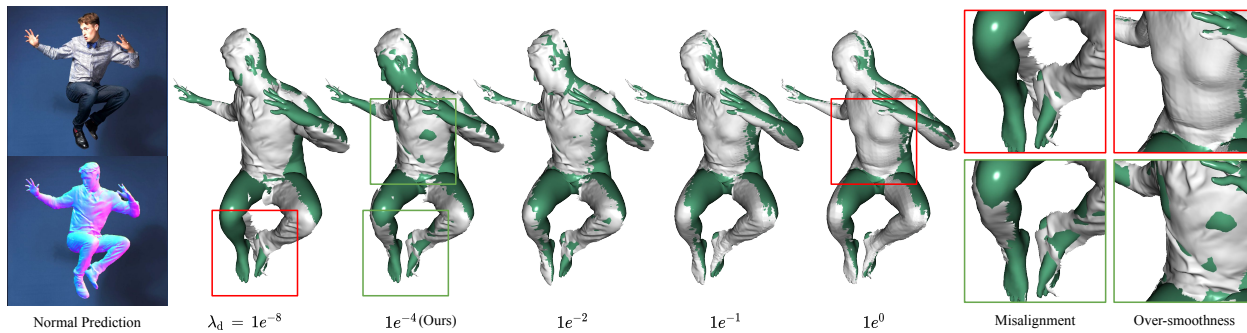


Figure A.4. **The effects of the hyperparameter λ_d on d-BiNI results.** λ_d controls how much d-BiNI surfaces agree with the SMPL-X mesh. A small λ_d causes a misalignment between the d-BiNI surface and the SMPL-X mesh, thus it produces stitching artifacts. An excessively large λ_d enforces d-BiNI to rely too heavily on SMPL-X, thus it smooths out the high-frequency details obtained from normals.

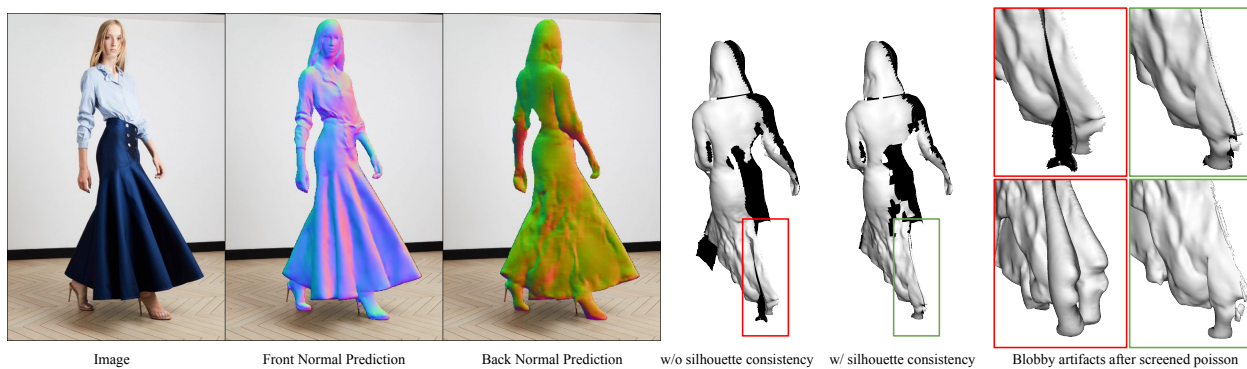


Figure A.5. **Necessity of silhouette consistency.** This term can be regarded as the mediator between front and back d-BiNI surfaces, preventing these surfaces from intersecting. Such intersection causes blobby artifacts after screened Poisson reconstruction [35].

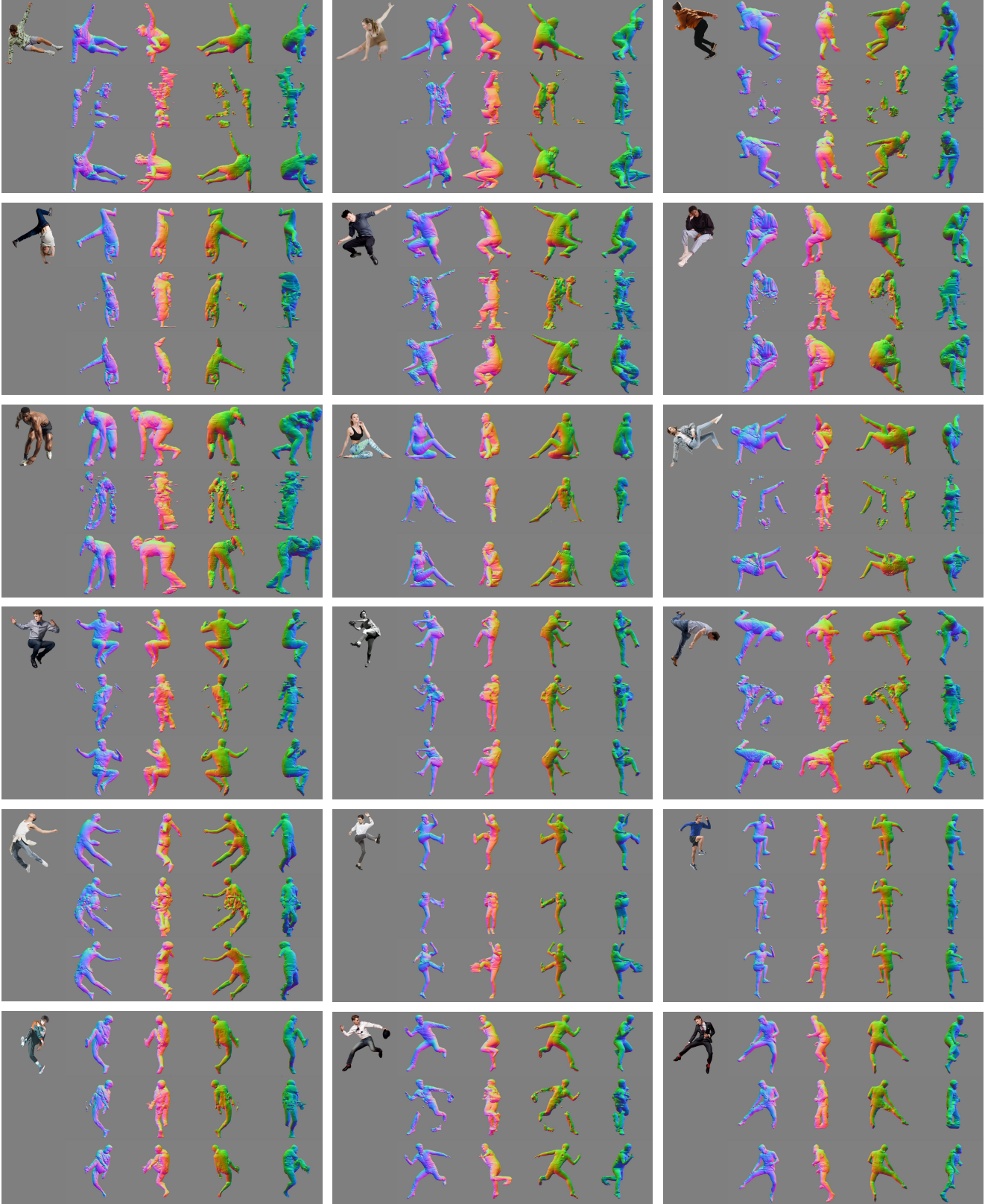


Figure A.6. **Results on in-the-wild images with challenging poses.** For each example (gray box) the format is as follows. **Top** \rightarrow **bottom**: ECON, PIFuHD [61] and ICON [67]. **Left** \rightarrow **right**: Virtual camera rotated by $\{0^\circ, 90^\circ, 180^\circ, 270^\circ\}$. **Q** Zoom in to see 3D details.

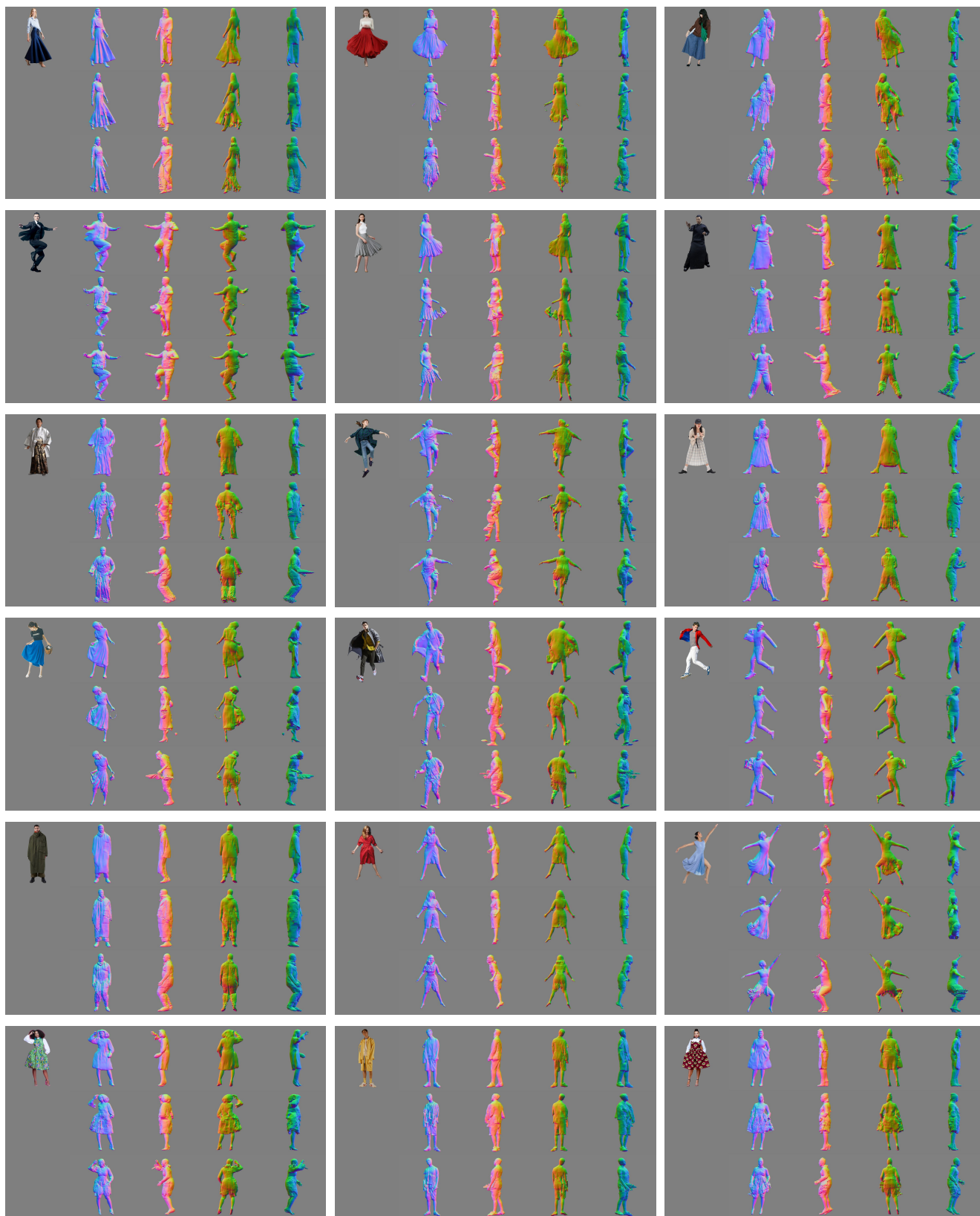


Figure A.7. **Results on in-the-wild images with loose clothing.** For each example (gray box) the format is as follows. **Top** \rightarrow **bottom**: ECON, PIFuHD [61] and ICON [67]. **Left** \rightarrow **right**: Virtual camera rotated by $\{0^\circ, 90^\circ, 180^\circ, 270^\circ\}$. **Q Zoom in** to see 3D details.

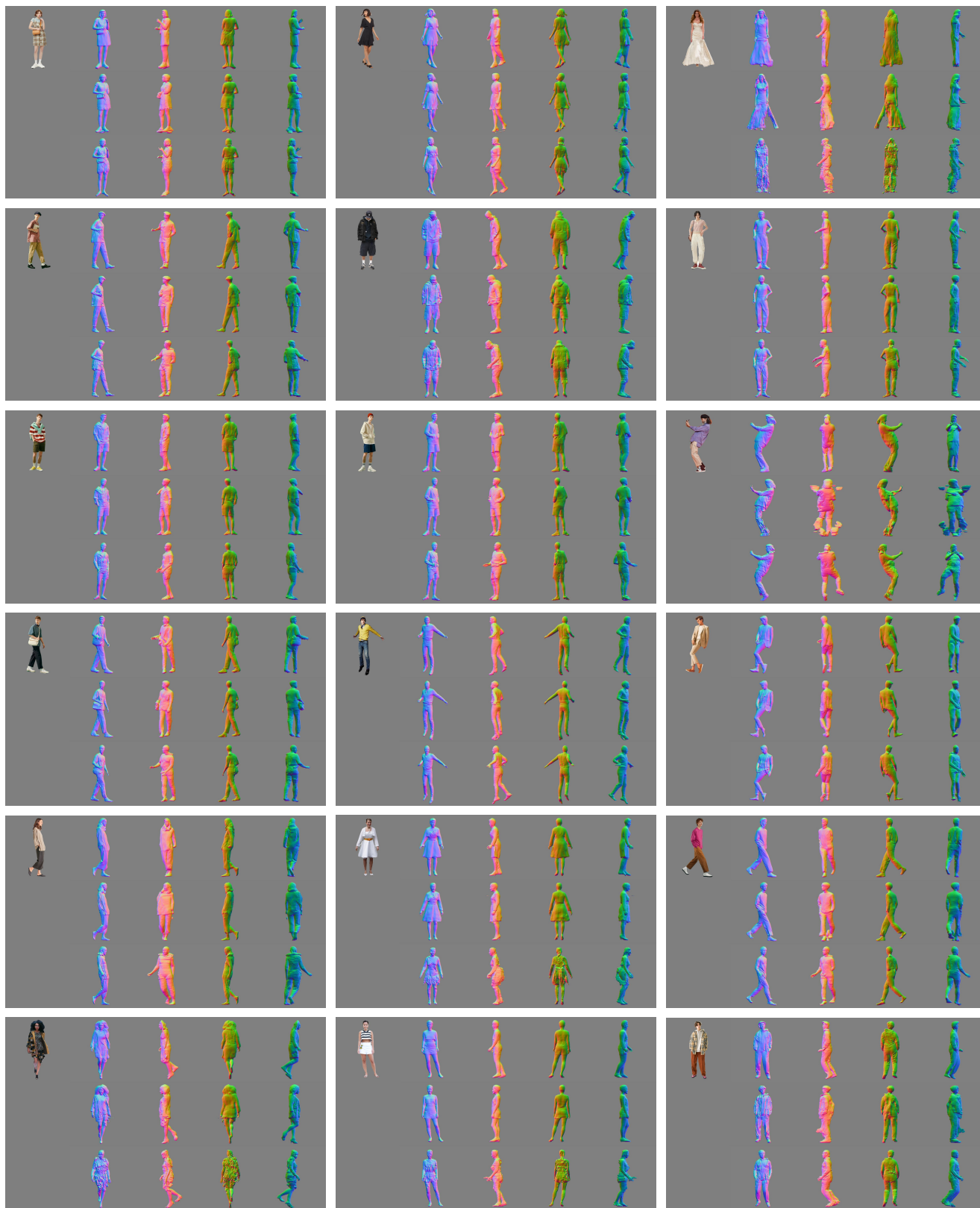


Figure A.8. **Results on in-the-wild fashion images.** For each example (gray box) the format is as follows. **Top** \rightarrow **bottom**: ECON, PIFuHD [61] and ICON [67]. **Left** \rightarrow **right**: Virtual camera rotated by $\{0^\circ, 90^\circ, 180^\circ, 270^\circ\}$. **Q** Zoom in to see 3D details.

References

- [1] HumanAlloy. humanalloy.com, 2018. 7
- [2] Thiemo Alldieck, Marcus A. Magnor, Bharat Lal Bhatnagar, Christian Theobalt, and Gerard Pons-Moll. Learning to reconstruct people in clothing from a single RGB camera. In *Computer Vision and Pattern Recognition (CVPR)*, 2019. 3
- [3] Thiemo Alldieck, Marcus A. Magnor, Weipeng Xu, Christian Theobalt, and Gerard Pons-Moll. Detailed human avatars from monocular video. In *International Conference on 3D Vision (3DV)*, 2018. 3
- [4] Thiemo Alldieck, Marcus A. Magnor, Weipeng Xu, Christian Theobalt, and Gerard Pons-Moll. Video based reconstruction of 3D people models. In *Computer Vision and Pattern Recognition (CVPR)*, 2018. 3
- [5] Thiemo Alldieck, Gerard Pons-Moll, Christian Theobalt, and Marcus A. Magnor. Tex2Shape: Detailed full human body geometry from a single image. In *International Conference on Computer Vision (ICCV)*, 2019. 3
- [6] XYZ. secure.axyz-design.com, 2018. 7
- [7] Alexander W Bergman, Petr Kellnhöfer, Yifan Wang, Eric R Chan, David B Lindell, and Gordon Wetzstein. Generative neural articulated radiance fields. In *Conference on Neural Information Processing Systems (NeurIPS)*, 2022. 7
- [8] Bharat Lal Bhatnagar, Garvita Tiwari, Christian Theobalt, and Gerard Pons-Moll. Multi-Garment Net: Learning to dress 3D people from images. In *International Conference on Computer Vision (ICCV)*, 2019. 3
- [9] Xu Cao, Hiroaki Santo, Boxin Shi, Fumio Okura, and Yasuyuki Matsushita. Bilateral normal integration. In *European Conference on Computer Vision (ECCV)*, 2022. 2, 4, 7, 9, 10, 11
- [10] Eric R. Chan, Connor Z. Lin, Matthew A. Chan, Koki Nagano, Boxiao Pan, Shalini De Mello, Orazio Gallo, Leonidas Guibas, Jonathan Tremblay, Sameh Khamis, Tero Karras, and Gordon Wetzstein. Efficient Geometry-aware 3D Generative Adversarial Networks. In *Computer Vision and Pattern Recognition (CVPR)*, 2022. 7
- [11] Xu Chen, Tianjian Jiang, Jie Song, Jinlong Yang, Michael J. Black, Andreas Geiger, and Otmar Hilliges. gDNA: Towards generative detailed neural avatars. In *Computer Vision and Pattern Recognition (CVPR)*, 2022. 2
- [12] Julian Chibane, Thiemo Alldieck, and Gerard Pons-Moll. Implicit functions in feature space for 3D shape reconstruction and completion. In *Computer Vision and Pattern Recognition (CVPR)*, 2020. 2, 3, 5, 7, 10
- [13] Julian Chibane, Aymen Mir, and Gerard Pons-Moll. Neural unsigned distance fields for implicit function learning. In *Conference on Neural Information Processing Systems (NeurIPS)*, 2020. 3
- [14] Vasileios Choutas, Lea Müller, Chun-Hao P. Huang, Siyu Tang, Dimitrios Tzionas, and Michael J. Black. Accurate 3D body shape regression via linguistic attributes and anthropometric measurements. In *Computer Vision and Pattern Recognition (CVPR)*, 2022. 3, 10
- [15] Enric Corona, Albert Pumarola, Guillem Alenyà, Gerard Pons-Moll, and Francesc Moreno-Noguer. SMPLicit: Topology-aware generative model for clothed people. In *Computer Vision and Pattern Recognition (CVPR)*, 2021. 3
- [16] Junting Dong, Qi Fang, Yudong Guo, Sida Peng, Qing Shuai, Xiaowei Zhou, and Hujun Bao. Totalselfscan: Learning full-body avatars from self-portrait videos of faces, hands, and bodies. In *Conference on Neural Information Processing Systems (NeurIPS)*, 2022. 8
- [17] Zijian Dong, Chen Guo, Jie Song, Xu Chen, Andreas Geiger, and Otmar Hilliges. PINA: Learning a personalized implicit neural avatar from a single RGB-D video sequence. In *Computer Vision and Pattern Recognition (CVPR)*, 2022. 3
- [18] Yao Feng, Vasileios Choutas, Timo Bolkart, Dimitrios Tzionas, and Michael J. Black. Collaborative regression of expressive bodies using moderation. In *International Conference on 3D Vision (3DV)*, 2021. 3, 4
- [19] Yao Feng, Jinlong Yang, Marc Pollefeys, Michael J. Black, and Timo Bolkart. Capturing and animation of body and clothing from monocular video. In *International Conference on Computer Graphics and Interactive Techniques (SIGGRAPH)*, 2022. 8
- [20] Jianglin Fu, Shikai Li, Yuming Jiang, Kwan-Yee Lin, Chen Qian, Chen Change Loy, Wayne Wu, and Ziwei Liu. StyleGAN-Human: A data-centric odyssey of human generation. In *European Conference on Computer Vision (ECCV)*, 2022. 7
- [21] Valentin Gabeur, Jean-Sébastien Franco, Xavier Martin, Cordelia Schmid, and Gregory Rogez. Moulding humans: Non-parametric 3D human shape estimation from single images. In *International Conference on Computer Vision (ICCV)*, 2019. 3, 5
- [22] Yuying Ge, Ruimao Zhang, Lingyun Wu, Xiaogang Wang, Xiaoou Tang, and Ping Luo. A Versatile Benchmark for Detection, Pose Estimation, Segmentation and Re-Identification of Clothing Images. *Computer Vision and Pattern Recognition (CVPR)*, 2019. 7
- [23] Artur Grigorev, Karim Isakov, Anastasia Ianina, Renat Bashirov, Ilya Zakharkin, Alexander Vakhitov, and Victor Lempitsky. Stylepeople: A generative model of fullbody human avatars. In *Computer Vision and Pattern Recognition (CVPR)*, 2021. 7
- [24] Kaiming He, Georgia Gkioxari, Piotr Dollár, and Ross Girshick. Mask r-cnn. In *International Conference on Computer Vision (ICCV)*, 2017. 9
- [25] Tong He, John P. Collomosse, Hailin Jin, and Stefano Soatto. Geo-PIFu: Geometry and pixel aligned implicit functions for single-view human reconstruction. In *Conference on Neural Information Processing Systems (NeurIPS)*, 2020. 2, 3
- [26] Tong He, Yuanlu Xu, Shunsuke Saito, Stefano Soatto, and Tony Tung. ARCH++: Animation-ready clothed human reconstruction revisited. In *International Conference on Computer Vision (ICCV)*, 2021. 3
- [27] Fangzhou Hong, Zhaoxi Chen, Yushi Lan, Liang Pan, and Ziwei Liu. EVA3D: Compositional 3D human generation from 2D image collections. *arXiv:2210.04888*, 2022. 7
- [28] Zeng Huang, Yuanlu Xu, Christoph Lassner, Hao Li, and Tony Tung. ARCH: Animatable reconstruction of clothed humans. In *Computer Vision and Pattern Recognition (CVPR)*, 2020. 3

- [29] Yasamin Jafarian and Hyun Soo Park. Learning High Fidelity Depths of Dressed Humans by Watching Social Media Dance Videos. In *Computer Vision and Pattern Recognition (CVPR)*, 2021. 2
- [30] Boyi Jiang, Yang Hong, Hujun Bao, and Juyong Zhang. Self-recon: Self reconstruction your digital avatar from monocular video. In *Computer Vision and Pattern Recognition (CVPR)*, 2022. 8
- [31] Boyi Jiang, Juyong Zhang, Yang Hong, Jinhao Luo, Ligang Liu, and Hujun Bao. BCNet: Learning body and cloth shape from a single image. In *European Conference on Computer Vision (ECCV)*, 2020. 3
- [32] Suyi Jiang, Haoran Jiang, Ziyu Wang, Haimin Luo, Wenzheng Chen, and Lan Xu. HumanGen: Generating Human Radiance Fields with Explicit Priors. *arXiv preprint:2212.05321*, 2022. 7
- [33] Hanbyul Joo, Tomas Simon, and Yaser Sheikh. Total capture: A 3D deformation model for tracking faces, hands, and bodies. In *Computer Vision and Pattern Recognition (CVPR)*, 2018. 3
- [34] Angjoo Kanazawa, Michael J. Black, David W. Jacobs, and Jitendra Malik. End-to-end recovery of human shape and pose. In *Computer Vision and Pattern Recognition (CVPR)*, 2018. 3
- [35] Michael Kazhdan and Hugues Hoppe. Screened poisson surface reconstruction. *Transactions on Graphics (TOG)*, 2013. 2, 5, 10, 11
- [36] Muhammed Kocabas, Nikos Athanasiou, and Michael J. Black. VIBE: Video inference for human body pose and shape estimation. In *Computer Vision and Pattern Recognition (CVPR)*, 2020. 3
- [37] Muhammed Kocabas, Chun-Hao P. Huang, Otmar Hilliges, and Michael J. Black. PARE: Part attention regressor for 3D human body estimation. In *International Conference on Computer Vision (ICCV)*, 2021. 3
- [38] Nikos Kolotouros, Georgios Pavlakos, Michael J. Black, and Kostas Daniilidis. Learning to reconstruct 3D human pose and shape via model-fitting in the loop. In *International Conference on Computer Vision (ICCV)*, 2019. 3
- [39] Verica Lazova, Eldar Insafutdinov, and Gerard Pons-Moll. 360-Degree textures of people in clothing from a single image. In *International Conference on 3D Vision (3DV)*, 2019. 3
- [40] Binh Le and Zhigang Deng. Smooth skinning decomposition with rigid bones. *Transactions on Graphics (TOG)*, 2012. 8
- [41] Jiefeng Li, Chao Xu, Zhicun Chen, Siyuan Bian, Lixin Yang, and Cewu Lu. HybrIK: A hybrid analytical-neural inverse kinematics solution for 3D human pose and shape estimation. In *Computer Vision and Pattern Recognition (CVPR)*, 2021. 3
- [42] Lei Li, Zhizheng Liu, Weining Ren, Liudi Yang, Fangjinhua Wang, Marc Pollefeys, and Songyou Peng. 3D textured shape recovery with learned geometric priors. *arXiv:2209.03254*, 2022. 5
- [43] Ruilong Li, Kyle Olszewski, Yuliang Xiu, Shunsuke Saito, Zeng Huang, and Hao Li. Volumetric human teleportation. In *SIGGRAPH Real-Time Live*, 2020. 9
- [44] Ruilong Li, Yuliang Xiu, Shunsuke Saito, Zeng Huang, Kyle Olszewski, and Hao Li. Monocular real-time volumetric performance capture. In *European Conference on Computer Vision (ECCV)*, 2020. 9
- [45] Zhe Li, Tao Yu, Chuanyu Pan, Zerong Zheng, and Yebin Liu. Robust 3D self-portraits in Seconds. In *Computer Vision and Pattern Recognition (CVPR)*, 2020. 3
- [46] Ziwei Liu, Ping Luo, Shi Qiu, Xiaogang Wang, and Xiaoou Tang. Deepfashion: Powering robust clothes recognition and retrieval with rich annotations. In *Computer Vision and Pattern Recognition (CVPR)*, 2016. 7
- [47] Matthew Loper, Naureen Mahmood, Javier Romero, Gerard Pons-Moll, and Michael J. Black. SMPL: A skinned multi-person linear model. *Transactions on Graphics (TOG)*, 2015. 2, 3
- [48] William E. Lorensen and Harvey E. Cline. Marching cubes: A high resolution 3D surface construction algorithm. *International Conference on Computer Graphics and Interactive Techniques (SIGGRAPH)*, 1987. 5
- [49] Camillo Lugaresi, Jiuqiang Tang, Hadon Nash, Chris McClanahan, Esha Uboweja, Michael Hays, Fan Zhang, Chuo-Ling Chang, Ming Guang Yong, Juhyun Lee, et al. Mediapipe: A framework for building perception pipelines. *arXiv:1906.08172*, 2019. 9
- [50] Qianli Ma, Jinlong Yang, Anurag Ranjan, Sergi Pujades, Gerard Pons-Moll, Siyu Tang, and Michael J. Black. Learning to dress 3D people in generative clothing. In *Computer Vision and Pattern Recognition (CVPR)*, 2020. 2, 6, 7
- [51] Lars M. Mescheder, Michael Oechsle, Michael Niemeyer, Sebastian Nowozin, and Andreas Geiger. Occupancy networks: Learning 3D reconstruction in function space. In *Computer Vision and Pattern Recognition (CVPR)*, 2019. 2, 3
- [52] Gyeongseok Moon, Hyeongjin Nam, Takaaki Shiratori, and Kyoung Mu Lee. 3D clothed human reconstruction in the wild. In *European Conference on Computer Vision (ECCV)*, 2022. 3
- [53] Atsuhiko Noguchi, Xiao Sun, Stephen Lin, and Tatsuya Harada. Unsupervised learning of efficient geometry-aware neural articulated representations. In *European Conference on Computer Vision (ECCV)*, 2022. 7
- [54] Jeong Joon Park, Peter Florence, Julian Straub, Richard A. Newcombe, and Steven Lovegrove. DeepSDF: Learning continuous signed distance functions for shape representation. In *Computer Vision and Pattern Recognition (CVPR)*, 2019. 2, 3
- [55] Georgios Pavlakos, Vasileios Choutas, Nima Ghorbani, Timo Bolkart, Ahmed A. A. Osman, Dimitrios Tzionas, and Michael J. Black. Expressive body capture: 3D hands, face, and body from a single image. In *Computer Vision and Pattern Recognition (CVPR)*, 2019. 2, 3
- [56] Gerard Pons-Moll, Sergi Pujades, Sonny Hu, and Michael J. Black. ClothCap: Seamless 4D clothing capture and retargeting. *Transactions on Graphics (TOG)*, 2017. 3
- [57] Yvain Quéau, Jean-Denis Durou, and Jean-François Aujol. Normal integration: A survey. *Journal of Mathematical Imaging and Vision*, 2018. 4
- [58] RenderPeople. renderpeople.com, 2018. 2, 6, 7

- [59] Javier Romero, Dimitrios Tzionas, and Michael J. Black. Embodied hands: Modeling and capturing hands and bodies together. *Transactions on Graphics (TOG)*, 2017. 3
- [60] Shunsuke Saito, Zeng Huang, Ryota Natsume, Shigeo Morishima, Hao Li, and Angjoo Kanazawa. PIFu: Pixel-aligned implicit function for high-resolution clothed human digitization. In *International Conference on Computer Vision (ICCV)*, 2019. 2, 3, 6
- [61] Shunsuke Saito, Tomas Simon, Jason M. Saragih, and Hanbyul Joo. PIFuHD: Multi-level pixel-aligned implicit function for high-resolution 3D human digitization. In *Computer Vision and Pattern Recognition (CVPR)*, 2020. 2, 3, 4, 6, 10, 12, 13, 14
- [62] David Smith, Matthew Loper, Xiaochen Hu, Paris Mavroidis, and Javier Romero. FACSIMILE: Fast and accurate scans from an image in less than a second. In *International Conference on Computer Vision (ICCV)*, 2019. 3, 5
- [63] Yu Sun, Wu Liu, Qian Bao, Yili Fu, Tao Mei, and Michael J. Black. Putting people in their place: Monocular regression of 3D people in depth. In *Computer Vision and Pattern Recognition (CVPR)*, 2022. 3
- [64] Yi Wang, Xin Tao, Xiaojuan Qi, Xiaoyong Shen, and Jiaya Jia. Image inpainting via generative multi-column convolutional neural networks. *Conference on Neural Information Processing Systems (NeurIPS)*, 2018. 3
- [65] Donglai Xiang, Fabian Prada, Chenglei Wu, and Jessica K. Hodgins. MonoClothCap: Towards temporally coherent clothing capture from monocular RGB video. In *International Conference on 3D Vision (3DV)*, 2020. 3
- [66] Yongqin Xiang, Julian Chibane, Bharat Lal Bhatnagar, Bernt Schiele, Zeynep Akata, and Gerard Pons-Moll. Any-Shot GIN: Generalizing implicit networks for reconstructing novel classes. In *International Conference on 3D Vision (3DV)*, 2022. 3
- [67] Yuliang Xiu, Jinlong Yang, Dimitrios Tzionas, and Michael J. Black. ICON: Implicit Clothed humans Obtained from Normals. In *Computer Vision and Pattern Recognition (CVPR)*, 2022. 2, 3, 4, 6, 9, 10, 12, 13, 14
- [68] Hongyi Xu, Eduard Gabriel Bazavan, Andrei Zanfir, William T. Freeman, Rahul Sukthankar, and Cristian Sminchisescu. GHUM & GHUML: Generative 3D human shape and articulated pose models. In *Computer Vision and Pattern Recognition (CVPR)*, 2020. 3
- [69] Ze Yang, Shenlong Wang, Sivabalan Manivasagam, Zeng Huang, Wei-Chiu Ma, Xinchen Yan, Ersin Yumer, and Raquel Urtasun. S3: Neural shape, skeleton, and skinning fields for 3D human modeling. In *Computer Vision and Pattern Recognition (CVPR)*, 2021. 2, 3
- [70] Tao Yu, Zerong Zheng, Kaiwen Guo, Pengpeng Liu, Qionghai Dai, and Yebin Liu. Function4D: Real-time human volumetric capture from very sparse consumer RGBD sensors. In *Computer Vision and Pattern Recognition (CVPR)*, 2021. 6, 7, 10
- [71] Ilya Zakharkin, Kirill Mazur, Artur Grigorev, and Victor Lempitsky. Point-based modeling of human clothing. In *International Conference on Computer Vision (ICCV)*, 2021. 3
- [72] Hongwen Zhang, Yating Tian, Yuxiang Zhang, Mengcheng Li, Liang An, Zhenan Sun, and Yebin Liu. PyMAF-X: Towards well-aligned full-body model regression from monocular images. *arXiv:2207.06400*, 2022. 3
- [73] Jianfeng Zhang, Zihang Jiang, Dingdong Yang, Hongyi Xu, Yichun Shi, Guoxian Song, Zhongcong Xu, Xinchao Wang, and Jiashi Feng. AvatarGen: A 3D generative model for animatable human avatars. In *arXiv:2208.00561*, 2022. 7
- [74] Yang Zheng, Ruizhi Shao, Yuxiang Zhang, Tao Yu, Zerong Zheng, Qionghai Dai, and Yebin Liu. DeepMultiCap: Performance capture of multiple characters using sparse multiview cameras. In *International Conference on Computer Vision (ICCV)*, 2021. 3
- [75] Zerong Zheng, Tao Yu, Yebin Liu, and Qionghai Dai. PaMIR: Parametric model-conditioned implicit representation for image-based human reconstruction. *Transactions on Pattern Analysis and Machine Intelligence (TPAMI)*, 2022. 2, 3, 6
- [76] Zerong Zheng, Tao Yu, Yixuan Wei, Qionghai Dai, and Yebin Liu. DeepHuman: 3D human reconstruction from a single image. In *International Conference on Computer Vision (ICCV)*, 2019. 7
- [77] Zhun Zhong, Liang Zheng, Guoliang Kang, Shaozi Li, and Yi Yang. Random erasing data augmentation. In *AAAI Conference on Artificial Intelligence*, 2020. 10
- [78] Hao Zhu, Xinxin Zuo, Sen Wang, Xun Cao, and Ruigang Yang. Detailed human shape estimation from a single image by hierarchical mesh deformation. In *Computer Vision and Pattern Recognition (CVPR)*, 2019. 3